# Characteristic low-temperature magnetic properties of aluminous goethite [α-(Fe, Al)OOH] explained

Qingsong Liu,[1] Yongjae Yu,[2] José Torrent,[3] Andrew P. Roberts,[1] Yongxin Pan,[4] and Rixiang Zhu[4]

[1] Goethite ($\alpha$-FeOOH) is an antiferromagnetic iron oxyhydroxide that forms as a weathering product of iron-bearing minerals. We systematically investigated the low- and room temperature properties of well-defined aluminous goethites [$\alpha$-(Fe, Al)OOH] with varying grain size and Al content. A marked decrease in the Néel temperature with increasing Al content for goethite lowers the blocking temperature distribution, which produces an increase in the remanent magnetization on cooling. The zero-field-cooled (ZFC) and field-cooled (FC) curves are irreversible. This is due to an additional partial thermal remanent magnetization (pTRM), which is acquired at low temperatures during the FC process because the initial 300 K remanence is far from being saturated due to the extremely high saturation field of goethite. This pTRM can be thermally demagnetized when reheating a sample back to 300 K. Finally, a sharp decrease in the bulk coercivity at 11–13 mol % Al is mostly caused by a broad coercivity distribution due to nonuniformity of Al substitution, which becomes more significant with increasing Al content. The positive correlation between pTRM acquisition during the FC process and the bulk coercivity strongly indicates that the ZFC/FC behavior is controlled by the bulk coercivity, which is, in turn, determined by Al substitution. This explanation of the characteristic low-temperature magnetic properties of Al goethite provides important constraints for identifying natural Al goethite bearing samples and quantitatively estimating the contributions of this mineral to the bulk magnetic properties of such samples.

## 1. Introduction

[2] Goethite ($\alpha$-FeOOH) is an antiferromagnetic iron oxyhydroxide that is commonly found in soils and sediments as a weathering product of iron-bearing minerals. Superimposed on the antiferromagnetic structure, goethite also possesses an additional weak parasitic, but hard, ferromagnetism below its Néel temperature ($T_N$), which is responsible for its paleomagnetic significance [e.g., *Banerjee*, 1970; *Hedley*, 1971; *Rochette and Fillion*, 1989; *Özdemir and Dunlop*, 1996]. The formation and preservation of goethite is highly sensitive to the soil environment [*Schwertmann*, 1985; *Balsam et al.*, 2004]. Therefore its presence can be indicative of soil forming conditions.

[3] The basic magnetic properties of both natural and synthetic goethite have been extensively investigated [*Strangway et al.*, 1967; 1968; *Banerjee*, 1970; *Dekkers*, 1988, 1989a, 1989b; *Rochette and Fillion*, 1989; *Pollard et al.*, 1991; *Özdemir and Dunlop*, 1996; *Mathé et al.*, 1999; *Guyodo et al.*, 2003; *Liu et al.*, 2004; *Rochette et al.*, 2005]. The spin coupling of goethite lies along the crystallographic $b$ axis (in the *Pnma* space group, Figure 1a), and defects or isomorphous cation substitutions (e.g., aluminum, Al) result in a net magnetic moment along the $b$ axis. Increasing Al contents decrease the unit cell size [*Schulze and Schwertmann*, 1984]. Varying Al contents also influence the other chemical and physical properties of goethite, such as crystal size and surface area, phosphate adsorption, color, $OH^-$ structure [*Schulze and Schwertmann*, 1984], and magnetic properties [*Liu et al.*, 2004].

[4] The presence of goethite in natural samples can be diagnosed by Mössbauer spectroscopy, X-ray diffraction analysis of magnetic extracts, reflectance spectrophotometry, and magnetic techniques [*France and Oldfield*, 2000; *Maher et al.*, 2004]. In particular, low-temperature magnetic properties can diagnose not only the presence of goethite in rocks and sediments but also the physical properties of the goethite. For example, the room temperature remanence

[1]National Oceanography Centre, University of Southampton, Southampton, UK.
[2]Department of Earth and Environmental Sciences, Korea University, South Korea.
[3]Departamento de Ciencias y Recursos Agrícolas y Forestales, Universidad de Córdoba, Córdoba, Spain.
[4]Institute of Geology and Geophysics, Chinese Academy of Sciences, Beijing, China.
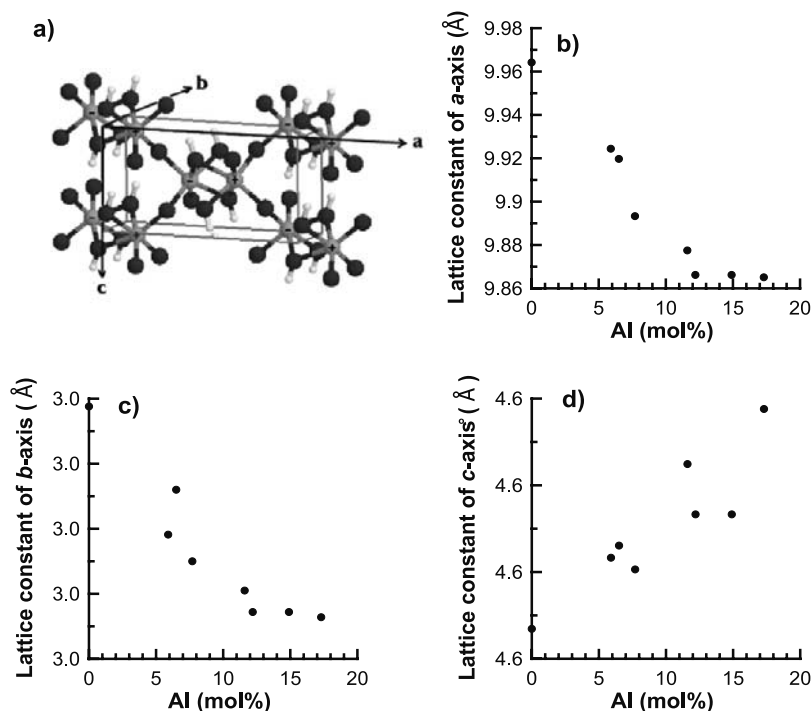
**Figure 1.** (a) Crystal structure of goethite. The larger and smaller light gray balls, and the darker gray balls represent Fe, H, and O atoms, respectively. The signs denote the antiferromagnetic coupling of iron atoms. Remanences are acquired along the $b$ axis. The notation is in the *Pnma* space group. Systematic variations of lattice constant as a function of Al mol % for the studied samples for the (b) $a$ axis, (c) $b$ axis, and (d) $c$ axis.

carried by goethite is highly enhanced upon cooling in a zero field, and the rate of increase of the remanence is strongly influenced by grain size and the degree of isomorphous cation substitution [*Dekkers*, 1989b; *Rochette and Fillion*, 1989; *Liu et al.*, 2004; *Maher et al.*, 2004]. However, the characteristic low-temperature behavior of goethite has not been fully explained.

[5] In this paper, we focus on unsolved questions associated with aluminous goethite in relation to the mechanism of (1) the enhancement of remanence intensity during cooling below the Néel and unblocking temperatures; (2) the large discrepancy between the zero-field-cooled (ZFC) and field-cooled (FC) curves; and (3) low-temperature hysteresis behavior. Our results provide an explanation for the low-temperature magnetic properties of goethite, as

well as providing important constraints on identification of goethite in natural samples.

## 2. Samples and Methods

[6] The synthesis process and properties of the Al goethites analyzed in this study are summarized in Tables 1 and 2. The studied samples were previously described by *Schulze and Schwertmann* [1984, 1987] and *Torrent et al.* [1987]. The Al mol % in the studied samples ranges from 0 to 17.3% (Table 2). X-ray diffraction (XRD) spectra demonstrate the presence of only goethite in the studied synthetic samples. This indicates good preservation of the sample and that no mineral transformations have occurred during the past two decades since the samples were originally synthesized.

**Table 1.** Methods Used to Synthesize the Studied Goethite Samples

| Sample | Procedure and Solutions Used | Alkali Added | Final [OH] or pH | Reference[a] |
|---|---|---|---|---|
| CB3 | 100 mL 1 $M$ Fe(NO$_3$)$_3$ + 0 to 75 mL 0.5 $M$ Al(NO$_3$)$_3$ at 323°C | 5 $M$ KOH | 0.6–1.2 | 1 |
| CB4 | 100 mL 1 $M$ Fe(NO$_3$)$_3$ + 0 to 75 mL 0.5 $M$ Al(NO$_3$)$_3$ at 298°C | 5 $M$ KOH | 0.6–1.2 | 1 |
| CB16 | 100 mL 1 $M$ Fe(NO$_3$)$_3$ + 0 to 75 mL 0.5 $M$ Al(NO$_3$)$_3$ | 3 $M$ KOH | 0.6–1.35 | 1 |
| CB11 | 100 mL 1 $M$ Fe(NO$_3$)$_3$ + 0 to 75 mL 0.5 $M$ Al(NO$_3$)$_3$ | 3 $M$ KOH | 0.6–1.35 | 1 |
| CB19 | 100 mL 1 $M$ Fe(NO$_3$)$_3$ + 0 to 75 mL 0.5 $M$ Al(NO$_3$)$_3$ | 3 $M$ KOH | 0.6–1.35 | 1 |
| CB22 | 200 mL 0.5 $M$ Fe(NO$_3$)$_3$ | 2 $M$ KOH | 0.9–1.35 | 1 |
| 34/7 | mixtures of Fe(NO3)$_3$ and AlCl$_3$ solutions stored for 14 days at 70°C | 0.3 M KOH | ~12 | 2 |
| 35/3 | 1.5 L 0.5 $M$ Al(NO$_3$)$_3$ + 900 mL 5 $M$ KOH + 225 mL 1 $M$ Fe(NO$_3$)$_3$ for 1310 days at 25°C | 5 $M$ KOH | ~12 | 2 |
| 35/5 | 1.5 L 0.5 $M$ Al(NO$_3$)$_3$ + 900 mL 5 $M$ KOH + 225 mL 1 $M$ Fe(NO$_3$)$_3$ for 1310 days at 25°C | 5 $M$ KOH | ~12 | 2 |
| 53/6 | solutions of Al(NO$_3$)$_3$, Fe(NO$_3$)$_3$, and KOH; detailed procedure not recorded | KOH | ~12 | - |
| 53/7 | solutions of Al(NO$_3$)$_3$, Fe(NO$_3$)$_3$, and KOH; detailed procedure not recorded | KOH | ~12 | - |
| 53/8 | solutions of Al(NO$_3$)$_3$, Fe(NO$_3$)$_3$, and KOH; detailed procedure not recorded | KOH | ~12 | - |
| GV3 | solutions of Fe(NO3)3 + 2 M KOH, stored for 30 days at 35°C | | 13 | 3 |

[a]1, *Torrent et al.* [1990]; 2, *Schulze and Schwertmann* [1987]; 3, *Torrent et al.* [1987].

**Table 2.** Summary of Physical and Magnetic Properties of the Studied Al Goethite Samples

| Sample | Al, mol % | $B_c$ at 20 K, mT | $B_c$ at 300 K, mT | Unit Cell Dimension, Å | | | $a*b*c$, Å³ | RI for IRM$_{100mT}$ | IRM$_{100mT}$, $10^{-5}$ A m²/g | $T_N$,[a] K |
| --- | --- | --- | --- | --- | --- | --- | --- | --- | --- | --- |
| | | | | c | a | b | | | | |
| CB19 | 17.3 | 375 | 2 | 4.638 | 9.865 | 2.996 | 137.087 | 6.58 | 0.119 | 311 |
| 53/8 | 14.9 | 415 | 88 | 4.613 | 9.866 | 2.997 | 136.420 | | | |
| CB4 | 12.9 | 350 | 100 | 4.580 | 9.880 | 2.998 | 135.682 | 4.23 | 6.974 | 328 |
| 53/7 | 12.2 | 580 | 315 | 4.613 | 9.866 | 2.997 | 136.420 | | | |
| 35/5 | 11.6 | 600 | | 4.625 | 9.878 | 3.001 | 137.070 | | | |
| 34/7 | 10.9 | 750 | 550 | | | | | 3.99 | 13.88 | 336 |
| 53/6 | 7.7 | 727 | 540 | 4.601 | 9.893 | 3.005 | 136.773 | | | |
| CB16 | 6.5 | | | 4.606 | 9.920 | 3.016 | 137.804 | 4.80 | 0.618 | 334 |
| Cb3 | 5.9 | 790 | 485 | 4.603 | 9.924 | 3.009 | 137.471 | 2.90 | 1.567 | 362 |
| 35/3 | 4.9 | 700 | 480 | | | | | 3.20 | 0.148 | 349 |
| CB22 | 0 | 249 | 80 | 4.587 | 9.964 | 3.029 | 138.431 | 1.93 | 0.018 | 380 |
| CB11 | 0 | 166 | | | | | | | | |
| GV3 | 0 | 157 | | | | | | | | |

[a]$T_N$ determinations are from *Liu et al.* [2004].

[7] Low-temperature experiments were conducted using a Quantum Designs Magnetic Properties Measurement System (MPMS). We characterized the temperature dependence of magnetic susceptibility ($\chi$-$T$) above room temperature to determine the Néel temperature. ZFC and FC curves, low-temperature cycle (LTC) and hysteresis measurements were made to determine the magnetic properties of the studied goethite samples at low temperatures. Magnetic susceptibility $\chi$-$T$ was measured using either an AC frequency of 1 kHz or a DC field of 0.35 mT. For ZFC and FC runs (the measured magnetization is denoted as $J_{ZFC-FC}$), the sample was first cooled from the initial temperature (denoted as $T_i$, which is $\leq$300 K) to 10 K in a zero field (ZFC). At 10 K, samples were subjected to a 2.5 T isothermal remanent magnetization (IRM) followed by warming to $T_i$ in the zero field, and subsequent cooling to 10 K (FC) in an applied field ($H_0$) of 2.5 T; the sample was finally warmed to $T_i$ in a zero field. To check how a partial thermal remanent magnetization (pTRM) was acquired during the FC process, sample CB16 was used to measure ZFC and FC curves with three different $T_i$ values at 300, 200, and 100 K, respectively. To address the effect of the applied field on the ZFC and FC behavior, the same sample CB16 was repeatedly subjected to ZFC and FC runs with $H_0$ of 10, 50, 100, 200, 500, and 2500 mT, respectively. The ratio of the magnetizations for the two curves ($J_{FC,10K}/J_{ZFC,10K}$) was used to quantify the differences between the ZFC and FC curves. The $H_0$ dependence of $J_{FC,10K}/J_{ZFC,10K}$ was then used to quantify the anisotropy constant ($H_K$) for the fraction of particles with unblocking temperatures below 300 K.

[8] For LTC experiments, an IRM was first imparted in a 2.5 T field at 300 K, followed by AF demagnetization at 100 mT. The remaining remanence (denoted as IRM$_{100mT}$) is a measurement of the hard fraction remanence, which is usually carried by hematite and goethite in natural samples [e.g., *Larrasoaña et al.*, 2003; *Liu et al.*, 2004]. The IRM$_{100\ mT}$ was then cycled between 300 and 20 K in zero field. The remanence increase (RI) upon cooling is defined as the ratio of $J_{20K}/J_{300K}$, where $J_{20K}$ and $J_{300K}$ are the remanences measured at 20 and 300 K, respectively. We also compared the $J_{20K}/J_{300K}$ parameter with the corresponding coercivity ($B_c$) measured at 300 K. All low-temperature measurements were made at steps of 2–5 K. The temperature sweep rate was 2 K/min with

corresponding errors less than ±0.5 K due to thermal lags while sweeping.

[9] The absolute value of RI also depends on the lowest temperature ($T_l$) used in the experiment. For example, previous studies with samples cooled to only 77 K ($-196°$C) [*Dekkers*, 1989b; *Maher et al.*, 2004], yielded a relatively lower RI. Note that we cooled samples to 20 K. The lower RI reported in previous studies is to be expected because the $M_s$ of goethite increases almost linearly with cooling so that RI will be lower at 77 K than it is at 20 K. Practically, to avoid the effects of $T_l$, RI can be further normalized as follows: (RI-1)/(300 K − $T_l$) (denoted as relative RI or RRI). Compared to RI, RRI is independent of $T_l$ and thus can be used to compare against different $T_l$ values.

[10] Hysteresis loops were measured for each sample at 300 and 20 K, respectively. The maximum $H_0$ was set to 5 T. To save time, the field increment was not kept constant, but was stepped from 1 mT ($H_0 \leq$ 10 mT), to 10 mT (10 mT < $H_0 \leq$ 100 mT), to 100 mT (100 mT < $H_0 \leq$ 1 T), and, finally, to 500 mT (1 T < $H_0 \leq$ 5 T).

[11] XRD spectra were measured using a Siemens D5005 X-ray diffractometer with a sealed tube, monochromatic Cu$K\alpha$ radiation. The scan speed was 0.005°2$\theta$ s$^{-1}$. Peaks for quartz (as an internal standard) were used to calibrate the XRD curves. The unit cell dimensions of goethite were calculated using the 110, 130, and 111 peaks [*Schulze and Schwertmann*, 1987]. Scanning electron microscope (SEM) observations were made using a LEO 1450VP SEM, operated at 10–20 keV with an acceleration voltage of 17–20 pA. Prior to observation, a small amount of sample ($\ll$1 mg) was diluted in about 5 ml of distilled water, and was then dispersed by ultrasonication. A drop of the suspension was then placed on a sample holder and allowed to dry in air. An Au coating was used to increase the conductivity of samples for high-resolution imaging. The grain sizes of Al goethite samples were estimated by measuring about 50–70 particles for each sample.

## 3. Results

[12] The unit cell size, determined from XRD analysis, versus the Al mol % of the studied Al goethite samples is shown in Figures 1b–1d. *Schulze and Schwertmann* [1984,
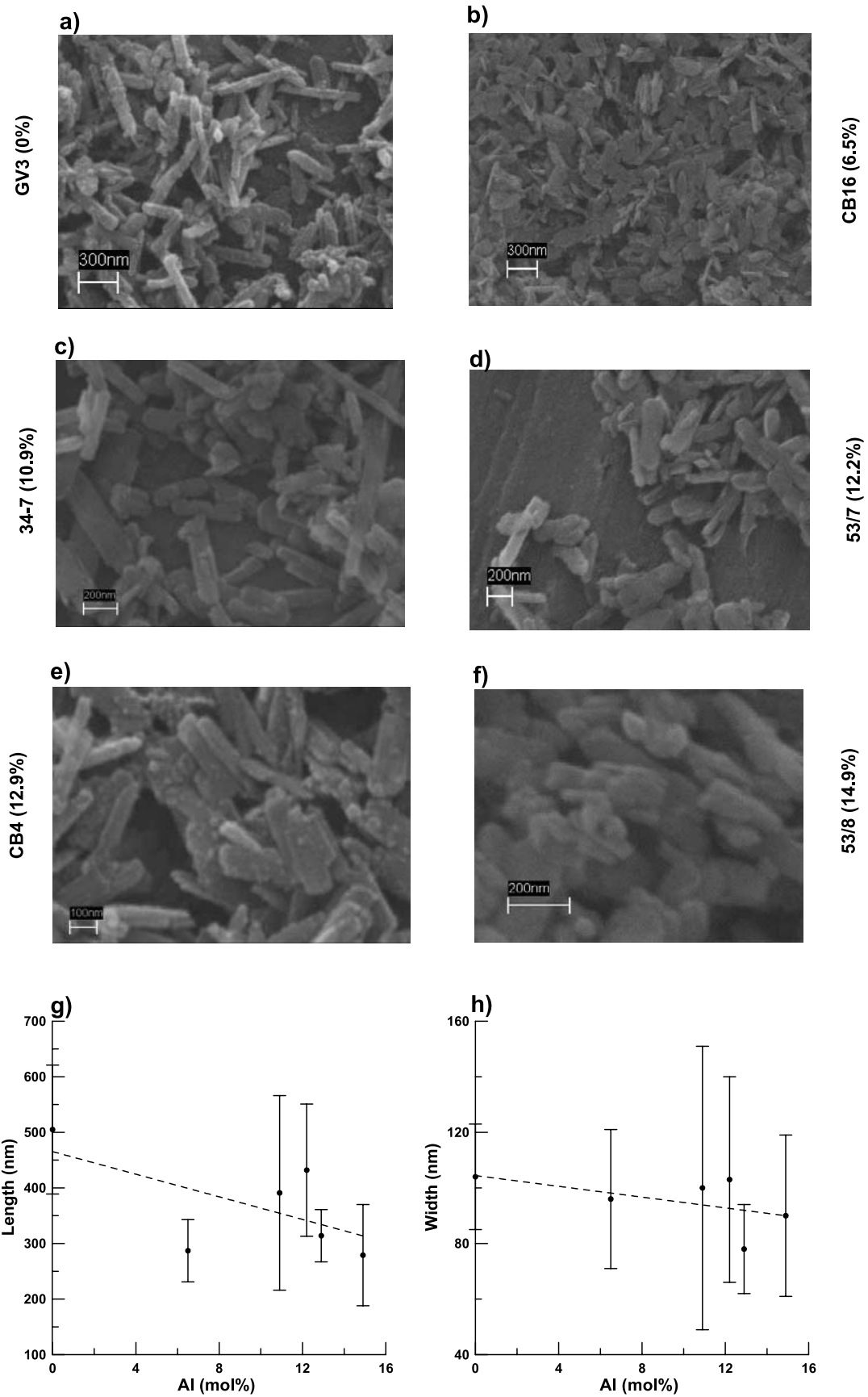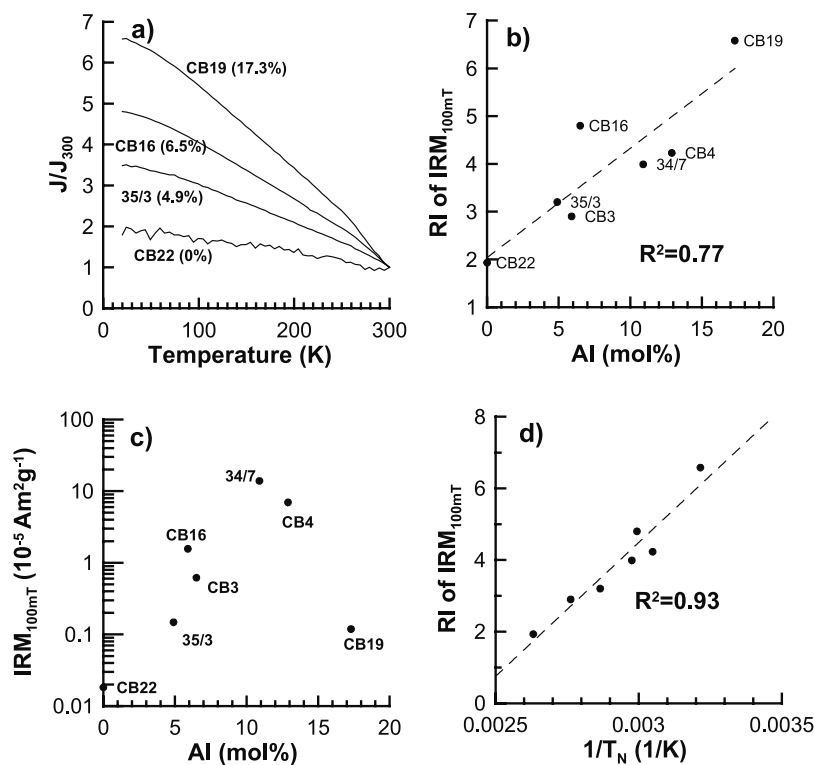
Figure 2

**Figure 3.** (a) Low-temperature cycle for selected aluminous goethite samples with different mol % Al substitution. (b) Remanence increase (RI, defined as the remanence intensity at 20 K normalized by the intensity at 300 K) for a room temperature $IRM_{100mT}$ for different Al contents. (c) Intensity of the room temperature $IRM_{100mT}$ for different Al contents (note that the $y$ axis has a logarithmic scale). (d) RI for a room temperature $IRM_{100mT}$ versus the reciprocal of the Néel temperature ($T_N$) [*Liu et al.*, 2004] for different Al contents (the dashed line is the linear trend for which the $R^2$ value applies).

1987] found that only the $a$ and $b$ crystallographic axes have a consistent negative correlation with Al mol %. On the other hand, the $c$ axis positively correlates with Al mol % (Figure 1d). Our results (Figure 1) are consistent with those of *Schulze and Schwertmann* [1984, 1987]. The unit cell size for both the $a$ and $b$ axes decreases with increasing Al content (Figures 1b and 1c), mainly because Al is smaller than Fe.

[13] SEM observations indicate that the grain sizes of the studied Al goethite samples vary greatly (Figure 2). The pure goethite grains (Al mol % = 0) have acicular shape (Figure 2a). With increasing Al substitution, the goethite grains generally become shorter (Figures 2a–2f). The grain size generally tends to decrease with increasing Al contents (Figures 2g and 2h), as observed by *Schulze and Schwertmann* [1987]. The secondary nonlinear grain size changes with respect to Al content differences are probably due to the use of different synthesis procedures to produce the different samples.

[14] Representative LTC behavior of $IRM_{100mT}$ for Al goethite is shown in Figure 3a. Upon cooling, the remanences are significantly enhanced and the corresponding RI

increases linearly with Al mol % (Figure 3b). The intensity of $IRM_{100mT}$ is positively correlated with Al mol % and reaches a maximum at ~11 mol % Al (sample 34/7), and then decreases for higher Al contents (Figure 3c). The RI is also linearly correlated with the inverse of $T_N$ (Figure 3d), which indicates that RI is strongly controlled by $T_N$, which is, in turn, controlled by the Al content (compare section 4.1). The fitted linear trends (Figures 3b and 3d) for RI and for the corresponding RRI versus Al mol % are

$$RI = 0.23 \times Al\ mol\ \% + 2.03, \tag{1}$$

$$RRI = 0.00082 \times Al\ mol\ \% + 0.00371. \tag{2}$$

[15] The ZFC/FC curves for the studied Al goethite samples vary significantly from sample to sample (Figure 4). However, a common feature is that all of the FC curves have stronger magnetizations than the corresponding ZFC curves. This indicates that samples acquired an additional remanence during the FC process. The difference between the ZFC and FC curves, as indicated by $J_{ZFC,10K}/J_{FC,10K}$, is

**Figure 2.** Back-scattered electron images of representative Al goethite samples: (a) GV3 (0 mol % Al), (b) CB16 (6.5 mol % Al), (c) 34/7 (10.9 mol % Al), (d) 53/7 (12.2 mol % Al), (e) CB4 (12.9% mol % Al), and (f) 53/8 (14.9 mol % Al). (g) and (h) Plots of the length and width of Al goethite samples versus mol % Al substitution, respectively. The vertical bars indicate the standard deviation. The grains tend to be less elongated with increasing Al substitution as shown by the approximately linear trends (dashed lines) in Figures 2g and 2h.
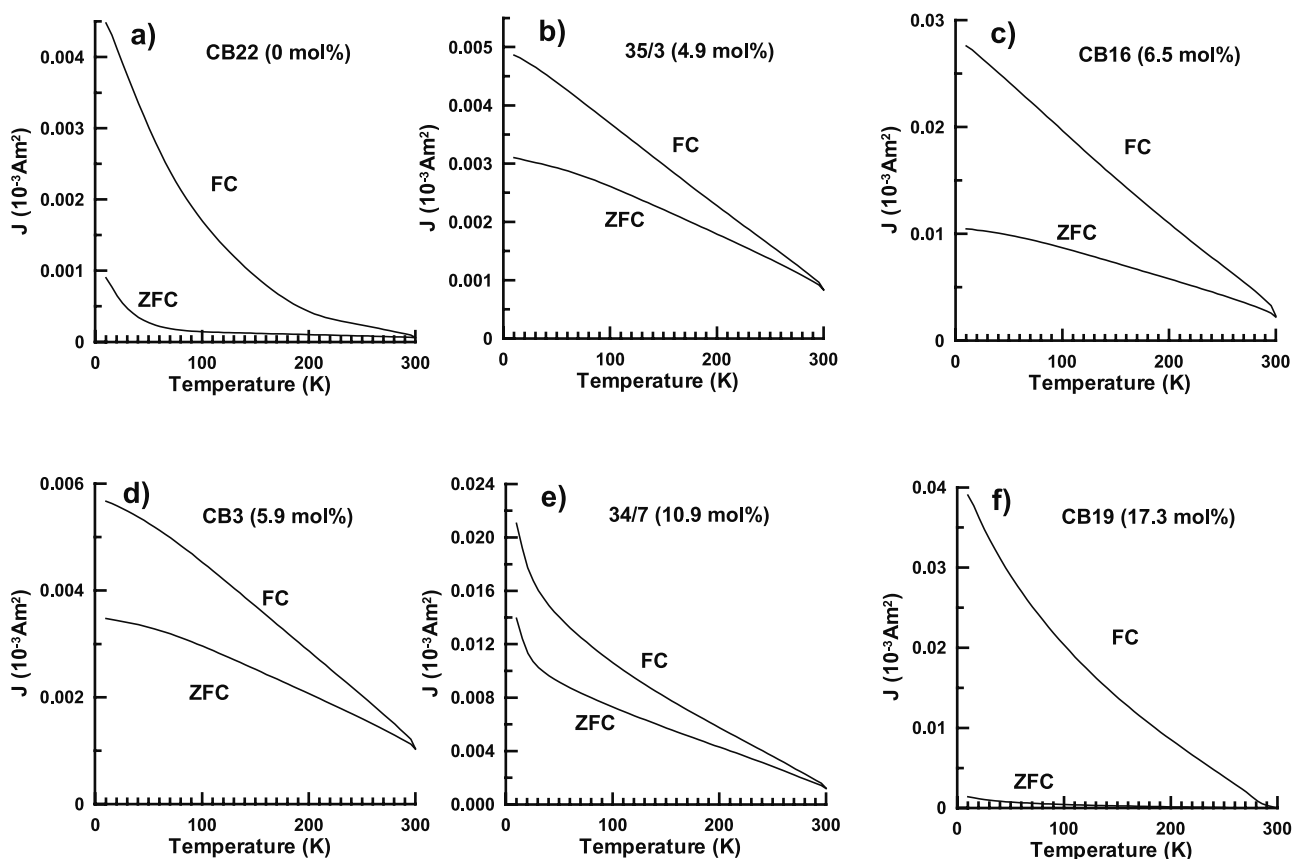
**Figure 4.** ZFC/FC warming curves for representative Al goethite samples. Numbers denote the Al mol %.

largest for the two end-member samples CB22 (pure goethite) and CB19 (17.3 Al mol %), and is lower for intermediate Al contents (Figure 4).

[16] The ZFC/FC curves have a strong initial state dependence (Figure 5). For $T_i$ below 200 K (Figures 5a and 5b), the ZFC and FC curves differ little. A large difference between the ZFC and FC curves is observed only when the initial temperature is raised to 300 K, which indicates that the additional remanence (in this case, it is a pTRM) is acquired only at temperatures above 200 K

(Figure 5c). Below 200 K, the almost repeatable ZFC and FC curves suggest that the remanence has been blocked and that no apparent pTRM can be acquired.

[17] To further understand the origin of the observed ZFC/FC behavior for aluminous goethite, the $H_0$ dependence of ZFC/FC curves for sample CB16 is shown in Figure 6. The FC curves are almost identical regardless of the strength of the applied field (Figure 6a). In contrast, the ZFC curves systematically change with applied field (Figure 6b). The $J_{ZFC,10K}/J_{FC,10K}$ ratio first decreases as the
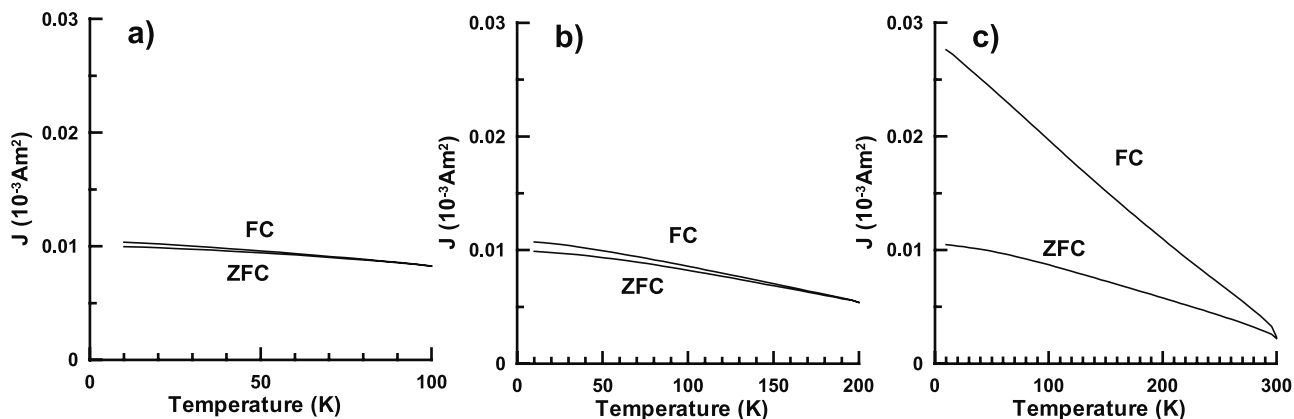


**Figure 5.** ZFC/FC curves for sample CB16 with different initial reference temperatures: (a) 100 K, (b) 200 K, and (c) 300 K.
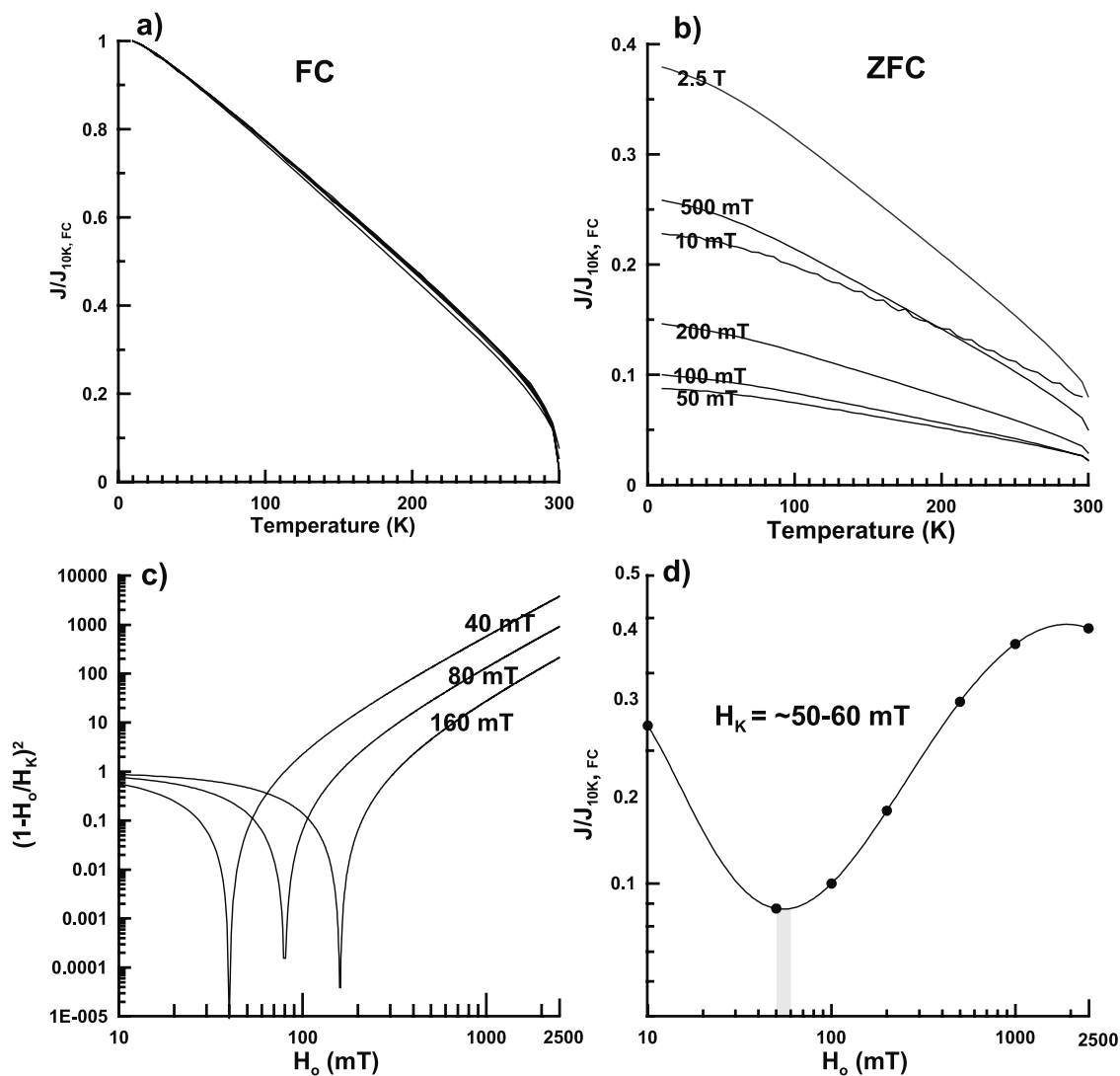
**Figure 6.** (a) and (b) FC and ZFC warming curves for different maximum applied fields. All curves have been normalized by the intensity of the FC curves at 10 K. The curves are individually labeled in Figure 6b, whereas in Figure 6a the curves are indistinguishable from each other. (c) Theoretical curves for the field dependence of $(1 - H_o/H_k)^2$, where $H_o$ and $H_k$ are the applied field and the anisotropy, respectively. (d) Field dependence of the normalized intensity $J/J_{10K}$ for sample CB16, where $J$ and $J_{10K}$ are the intensities of the ZFC and FC warming curves at 10 K, respectively. The gray bar in Figure 6d marks the minimum of $J/J_{10K}$, which corresponds to $H_k$.

applied field increases from 10 to 50 mT, but it then steadily increases with further increases in the applied field (Figure 6b). Three theoretical curves of $(1 - H_0/H_K)^2$ are illustrated for $H_0 = 40$, 80, and 160 mT (Figure 6c). Physical interpretation of these curves is provided in section 4.2.

[18] Hysteresis loops for the studied Al goethites are illustrated in Figure 7. None of the samples are magnetically saturated at the maximum applied field of 5 T. These loops are therefore only partial hysteresis loops. The second dominant feature is the "wasp-waisted" nature of the loops, especially for the 20 K loops, which indicates that the synthetic samples consist of a mixture of grains with different sizes and coercivities [*Roberts et al.*, 1995]. The nonuniform nature of the grain size distribution is partially supported by the electron micrographs (Figure 2), e.g., for

samples 53/7 and 53/8, which have strongly wasp-waisted hysteresis loops. The coercivity can also be strongly affected by Al content due to nonuniform Al substitution even if the grain size distribution is uniform.

[19] The dependence of coercivity on Al mol %, as measured at 20 and 300 K, is shown in Figure 8a. It should be noted that the 5 T maximum fields used are insufficient to magnetically saturate the samples, so the coercivity dependence discussed below concerns the coercivity of partial hysteresis loops. Overall, the low- and room temperature coercivities have similar trends with respect to Al mol %. The coercivity sharply increases between 0 and ~6 Al mol %. A nearly constant coercivity is observed between ~6 and ~11 Al mol %. Above ~11 mol %, the coercivity sharply decreases (Figure 8a). However, at 20 K the
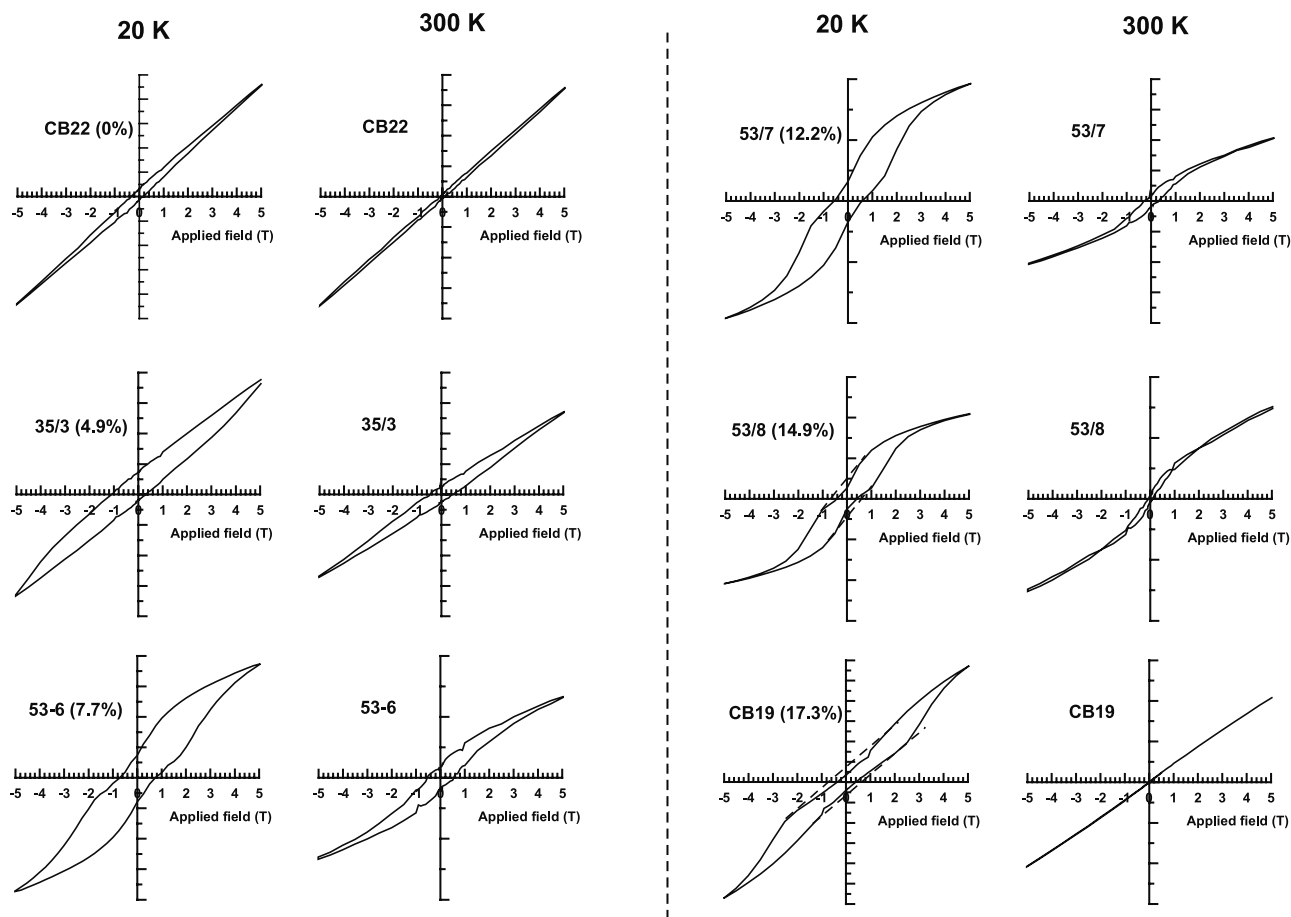
**Figure 7.** Hysteresis loops measured at 20 K and 300 K for the studied Al goethite samples. The dashed lines denote the background trends determined using the values at applied field >1.5 T.

coercivities decrease only by ∼50%, while at 300 K the coercivities are reduced to almost zero for sample CB19. The $J_{ZFC,10K}/J_{FC,10K}$ ratio (rectangles on Figure 8a) has similarities compared to the trend of $B_c$ at 20 K, which indicates that the ZFC/FC behavior is strongly influenced by the coercivity.

[20] The relatively smaller coercivity of three pure goethite samples synthesized using two different processes compared to the Al-substituted goethite samples demonstrates that a slight increase in Al content can significantly increase the bulk coercivity. Room temperature coercivity values for pure goethite samples synthesized using other procedures are necessary to completely confirm this conclusion. There are no transitional features evident between 0 and ∼6 Al mol % in Figure 8a; therefore we focus more on the coercivity results for samples with Al mol % >∼6 mol % in the following discussion.

## 4. Discussion

### 4.1. Low-Temperature Magnetic Properties of Aluminous Goethite

[21] The large but reversible increase of the room temperature remanent magnetization of goethite upon cooling at low temperatures has been repeatedly reported [*Heller*, 1978; *Dekkers*, 1989b; *Rochette and Fillion*, 1989; *Maher*

*et al.*, 2004]. This reversibility indicates that the large changes in remanence are not caused by a wide distribution of blocking temperatures [*Rochette and Fillion*, 1989]. *Dekkers* [1989b] further reported an increase of RI with increasing degree of goethite impurity, and proposed that to first order this effect is due to the rise of $M_s$ with decreasing temperature. *Dekkers and Rochette* [1992] used fields up to 15 and 20 T in an effort to magnetically saturate their goethite samples. More recently, *Rochette et al.* [2005] investigated the high-field behavior of pure goethite up to about 60 T. They found that pure goethite does not saturate even at such high fields. In conventional experiments, in which the applied field is generally less than 3−5 T, goethite is far from being saturated, and will only acquire several percent of the expected SIRM [*Rochette et al.*, 2005]. Conventional techniques therefore underestimate the contribution of goethite to the bulk laboratory-induced remanence. Compared to the high-saturation field, the magnetic properties of goethite investigated in most studies represent only a "weak-field" remanence, despite the fact that fields of 1 T can saturate most ferrimagnetic minerals. For such weak remanences of the type investigated in the majority of studies, zero field LTC behavior is mostly controlled by the temperature dependence of saturation magnetization ($M_s$).
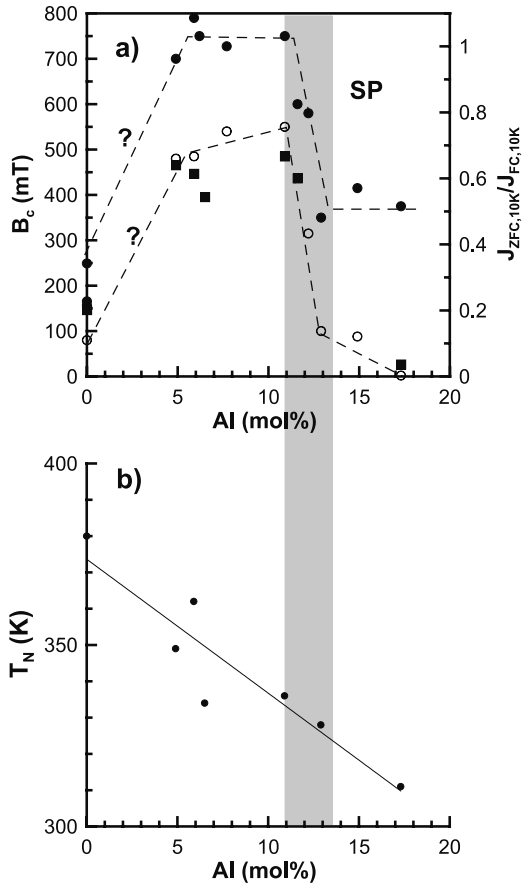
**Figure 8.** (a) Comparisons of $B_c$ at 20 K (solid circles) and 300 K (open circles), and $J_{ZFC,10K}/J_{FC,10K}$ (solid rectangles) for the studied Al goethite samples. Dashed lines indicate the trends with respect to Al mol %. (b) Correlation between $T_N$ and Al mol % for the studied Al goethite samples [*Liu et al.*, 2004]. The gray bar marks the coercivity transition at ~11–13 mol % Al.

Because $M_s$ is reversible, the corresponding weak-field remanence should also be reversible.

[22] Practically, the $M_s$ of goethite cannot be directly measured because of its large saturation field. Nevertheless, neutron diffraction data indicate that temperature-dependent $M_s$ curves of Al goethites with Al mol % up to 24.7% have identical features when plotted versus the reduced temperature $T/T_N$ [*Kilkoyne and Ritter*, 1997]. For pure goethite, $T_N = \sim400$ K, therefore the initial point at 300 K corresponds to $300/400 = 0.75$. When increasing the Al mol %, the $T_N$ of Al goethite decreases, resulting in an increase of the 300 K/$T_N$ ratio. Thus, although all the samples were measured in low-temperature cycles between 300 K and 20 K, they correspond to different initial states in terms of the $M_s \sim T/T_N$ curve because $T_N$ is different for the different Al goethite samples (RI is the ratio of $M_s$ at 20 K/$T_N$ to that at 300 K/$T_N$) [*Liu et al.*, 2004]. This observation can reasonably explain some basic aspects about RI: (1) RI is positively correlated with Al mol % [*Dekkers*, 1989b], and (2) it is controlled by the temperature interval between 300 K and the maximum unblocking temperature of goethite.

[23] For natural goethite, RI tends to decrease with increasing grain size [*Dekkers*, 1989b; *Maher et al.*, 2004]. It is likely that the inherent concentration of vacancies tends to decrease with increasing grain size of goethite, thus increasing $T_N$ and $T_b$ to higher temperatures, which, in turn, lowers RI. The absolute value of RI also depends on the lowest temperature used in the experiment. For example, previous studies with samples cooled to only 77 K (−196°C) [*Dekkers*, 1989b; *Maher et al.*, 2004], yielded a relatively lower RI.

### 4.2. Explanation of ZFC/FC Behavior for Aluminous Goethite

[24] Although all goethite samples exhibit large differences between their ZFC and FC curves at low temperatures, the curves converge at 300 K. This can expressed as

$$\mathrm{IRM_{FC}}(T) = \mathrm{IRM_{ZFC}}(T) + \mathrm{pTRM_{FC}}(T), \qquad (3)$$

where $\mathrm{IRM_{FC}}$ and $\mathrm{IRM_{ZFC}}$ are the IRM values for the FC and ZFC processes, and $\mathrm{pTRM_{FC}}$ is the partial TRM acquired when applying a field during the FC process. This equation is not valid for minerals such as magnetite or maghemite because their $\mathrm{IRM_{FC}}$ and $\mathrm{IRM_{ZFC}}$ curves are both saturated at $H_0$ values of 2.5 T. In contrast, for goethite, due to its large saturation field [*Rochette et al.*, 2005], a $\mathrm{TRM_{FC}}$ that is applied in most laboratory experiments (e.g., at 2.5 T) can be completely thermally demagnetized when warmed back to 300 K. Thus $\mathrm{IRM_{FC}}(300\ \mathrm{K}) = \mathrm{IRM_{ZFC}}(300\ \mathrm{K})$, and $\mathrm{pTRM_{FC}}(300\ \mathrm{K}) = 0$.

[25] As shown in Figure 5, $\mathrm{IRM_{FC}}(T)$ is enhanced only during cooling from temperatures just below the unblocking temperature (e.g., 300 K rather than 100 K or 200 K); the $\mathrm{IRM_{FC}}(T)$ and $\mathrm{IRM_{ZFC}}(T)$ curves replicate each other when the initial temperature is far below the unblocking temperature. This strongly confirms that the enhanced remanence is a TRM.

[26] $T_b$ and TRM behavior are strongly affected by the applied field, $H_0$ and can be expressed as [*Dunlop and Özdemir*, 1997]

$$\frac{T_b}{\beta^2(T_b)} = \left(\frac{\mu_0 V M_{S0} H_{K0}}{2k \ln(t/\tau_0)}\right)\left[1 - \frac{|H_0|}{H_{K0}\beta(T_b)}\right]^2, \qquad (4)$$

where $M_{s0}$ and $H_{K0}$ are $M_s$ (saturation magnetization) and $H_K$ (the anisotropy constant) at temperature $T_0$, $\beta(T) = M_s(T)/M_{s0}$, $V$ is the particle volume, $k$ is the Boltzmann constant ($1.38 \times 10^{-23}$ J/K), and $t$ is the measurement time (about 60 s). On the basis of equation (4), $T_b$ is quadratically correlated to $H_0$. For example, when $H_0$ is less than $H_K$, $T_b$ decreases with increasing $H_0$ [*Dunlop*, 1982]. A higher proportion of magnetic particles then becomes unblocked and can acquire a TRM during field cooling. Thus the FC curve will be further enhanced compared to the corresponding ZFC curve because more pTRM has been acquired. This will yield a lower $J_{ZFC,10K}/J_{FC,10K}$ ratio. In contrast, when $H_K < H_0$, an opposite trend will be observed so that $T_b$ will increase with further increasing $H_0$, and fewer particles with $T_b < 300$ K can acquire a TRM during the FC process, which will increase $J_{ZFC,10K}/J_{FC,10K}$ values. Therefore the

minimum of $J_{ZFC,10K}/J_{FC,10K}$ indicates $H_K$ for a portion of particles with $T_b < 300$ K. For sample CB16, the average $H_K$ value is estimated to be about 50–60 mT (Figure 6d). We would normally expect $H_K$ to be much larger for goethite; it makes intuitive sense that this estimate applies to the portion of grains that contribute to the TRM acquired at 300 K because it is the lowest coercivity particles that are most likely to be aligned at fields well below the saturating field. Note that the applied field used in this study is much smaller than the expected coercivity. Therefore only a small proportion of goethite particles with small $H_K$ is expected to be involved, the proportion with much larger coercivity values is "unseen" by the relatively small applied field. Therefore the $H_K$ value estimated from Figure 6d represents only the proportion of grains with small $H_K$. Theoretically, we expect very large $H_K$, then by integrating these two arguments together, we conclude that the goethite samples used in this study contain a wide range of coercivities (to the first order, the simplest case is a bimodal coercivity distribution).

[27] The ZFC/FC behavior will be determined by both the distribution of $T_b$, and the applied field, $H_0$. If a goethite sample has a narrow $T_b$ distribution with $T_b > 300$ K, then we predict that ZFC/FC curves for this sample will be nearly repeatable because less TRM can be acquired below 300 K. This is exactly the case for sample CB16 when the initial temperature is much lower than 300 K (Figures 5a and 5b). Therefore the prerequisites for a large difference between ZFC and FC curves for goethite are that (1) the initial remanence at 300 K is not saturated and (2) there is a fraction of particles with $T_b < 300$ K (Figure 5c).

[28] The large differences in the ZFC/FC curves among the studied samples could also be caused by a broad distribution of grain size and/or coercivity, as suggested by the wasp-waisted hysteresis loops [cf. *Roberts et al.*, 1995]. However, the hysteresis loop for sample CB22 is not wasp-waisted (Figure 7), but it does have a much lower $J_{ZFC,10K}/J_{FC,10K}$ value that is comparable to that of sample CB19, which produced a wasp-waisted loop at 20 K. Therefore a broad grain size distribution alone cannot explain the observed ZFC/FC behavior for the Al goethite samples.

[29] The strong correlation between $J_{ZFC,10K}/J_{FC,10K}$ and coercivity for the studied Al goethite samples (Figure 8a) demonstrates that the ZFC/FC behavior is controlled by the bulk coercivity. Goethite particles with lower coercivities are more likely to be in an unblocked state at room temperature, which will therefore enable them to acquire more pTRM during the ZFC process, which, in turn, decreases the $J_{ZFC,10K}/J_{FC,10K}$ ratio. *Dekkers* [1989a] documented that the room temperature coercivity of natural goethite first increases with increasing isomorphous cation substitution, and that it then decreases with a further rise in the amount of impurities. He proposed that the decrease in coercivity is probably due to the decrease of $T_b$. Our synthetic samples display similar room temperature and low-temperature behavior. For acicular single domain magnetite particles, the coercivity can reach up to ∼300 mT (= 0.5 × 480,000 A/m) due to shape anisotropy [*Dunlop and Özdemir*, 1997]. Although the studied Al goethite crystals also have elongated shape, their large coercivity values cannot be controlled by shape anisotropy because of

their much lower $M_s$ (which is about 2 orders of magnitude lower than magnetite). Instead, the large initial coercivities for Al contents of ∼4–14% arise from the magnetoelastic anisotropy due to internal stress [*Dunlop and Özdemir*, 1997]. When $M_s$ is low, coercivity ($B_c$) due to magnetoelastic anisotropy will be highly enhanced because for this case, $B_c$ is inversely proportional to $M_s$.

[30] When Al mol % is about 12%, the coercivity of the Al goethite samples sharply decreases (Figure 8a). This is not caused by variations in $T_N$ because $T_N$ is still well above room temperature, and there is no sharp change in $T_N$ at 12 mol % Al (Figure 8b). Therefore any effects due to $T_N$ should be reduced, especially for measurements at 20 K. Instead, this transition at ∼12 mol % Al appears to be mainly due to the effects of the wasp-waisted shape of the hysteresis loops (Figure 7), which are caused by the broad coercivity distribution (the simplest case is a bimodal distribution) [cf. *Roberts et al.*, 1995]. The wide coercivity distribution can be further demonstrated by Figure 6d. $J/J_{10\,K}$ for sample CB16 systematically changes with applied field $H_0$. The minimum at about 50–60 mT indicates an anisotropy constant. This value is much lower than the expected bulk coercivity (∼500 mT) at 300 K. Therefore the most reasonable interpretation is that this sample has a broad coercivity distribution resulting from increased imperfections and nonuniformity with increased Al content.

[31] For samples 53/8 (Al mol % = 14.9%) and CB19 (Al mol % = 17.3%) (Figure 7), we used linear trends to estimate the coercivity for the background hysteresis loops (see dashed lines in Figure 7). The coercivity is estimated to be about 800 mT for both of these samples, which is comparable to the coercivity values for samples with Al contents <12 mol %. This suggests that the sharp decrease in coercivity at around 12 mol % Al could be controlled by the lower coercivity fraction probably due to the nonuniform Al substitution.

## 4.3. Application to Quantitative Mineral Identification

[32] The extremely high-saturation field (above about 60 T) and relatively low $T_N$ (<400 K) make goethite unique in terms of its low-temperature properties. For conventional low-temperature measurements, the applied field is of the order of several tesla. Ferrimagnetic minerals can be easily saturated in such applied fields. Although hematite also has much higher coercivity than ferrimagnetic minerals, temperatures below 300 K are far below its $T_N$. Rather than the magnetic properties being controlled by the large increase of remanence upon cooling to low temperatures, magnetite and hematite undergo the Verwey and Morin transitions, respectively. The combination of the large discrepancy between the FC and ZFC curves, and the large and reversible increase in remanence upon cooling, are therefore diagnostic of the presence of goethite. The contrast in the low-temperature behavior between goethite and hematite can be further used to separate their contributions to the high-coercivity fraction of remanence (e.g., the "hard" IRM (HIRM) or IRM$_{100mT}$). *Maher et al.* [2004] and *Liu et al.* [2004] independently proposed the use of the low-temperature dependence of the hard IRM (HIRM) to identify and quantify goethite concentrations. Similar to IRM, the HIRM carried by goethite also increases upon

cooling. However, for natural sediments or soils containing goethite, the RI of HIRM will be positively correlated to both the concentration and mol % of isomorphous cation substitution. For a certain environment, if the amount of substitution is relatively constant, the RI of HIRM could be useful to quantify the concentration of goethite, and vice versa. The RI of HIRM can also be caused by ultrafine-grained hematite with $T_b$ just above 300 K [*Maher et al.*, 2004]; in this case, thermal instability at elevated temperatures could be used to distinguish between the presence of hematite and goethite.

[33] In natural samples, goethite usually co-occurs with hematite, and the corresponding RI values for bulk samples will be reduced. A more feasible solution to decouple the contributions of goethite and hematite is first to determine the unblocking temperature of Al goethite by high-temperature analysis, then to estimate the Al mol % on the basis of comparison with results from synthetic samples [e.g., *Liu et al.*, 2004]. Once the Al mol % is estimated, the expected RI (RI$_{\mathrm{exp}}$) can be calculated based on equation (1). The remanence carried by fine-grained hematite changes little upon cooling; therefore the hematite contribution ($J_{\mathrm{Hem}}$) to the initial remanence can be estimated by

$$\frac{J_{\mathrm{10K}} - J_{\mathrm{Hem}}}{J_{\mathrm{300K}} - J_{\mathrm{Hem}}} = \mathrm{RI_{Exp}}. \qquad (5)$$

This technique provides a practical way to quantify goethite contents in natural samples.

## 5. Conclusions

[34] Goethite has characteristic low-temperature magnetic properties due to its extremely high saturation field and low $T_b$. With increasing Al mol %, goethite undergoes a decrease in $T_N$ and $T_b$. When the initial temperature in a low-temperature cooling measurement cycle is fixed at 300 K, the 300 K/$T_N$ ratio increases with increasing Al contents. This is the main reason for the positive correlation between the remanence increase at low temperatures and Al mol %. Moreover, a typical applied field of several tesla cannot saturate the remanence at 300 K. Thus goethite can acquire an additional pTRM during the FC process, which will be thermally demagnetized when warming samples back to 300 K. Therefore the large differences between ZFC and FC curves and the large increase of the 300 K remanence upon cooling are diagnostic of the presence of goethite within a sample. In addition, the ZFC/FC behavior differs greatly among Al goethite samples with different Al contents. This is mainly due to variations in the bulk coercivity, which directly determine how much pTRM can be gained during the FC process. Finally, we propose several quantitative relationships between low-temperature magnetic properties and the Al mol % for Al goethite samples. These relationships have considerable potential to quantify goethite contents in natural samples, and thus have important implications for paleomagnetic and rock magnetic investigations of goethite-bearing samples.

## References

Balsam, W., J. Ji, and J. Chen (2004), Climatic interpretation of the Luochuan and Lingtai loess sections, China, based on changing iron oxide mineralogy and magnetic susceptibility, *Earth Planet. Sci. Lett.*, *223*, 335–348.

Banerjee, S. K. (1970), Origin of thermoremanence in goethite, *Earth Planet. Sci. Lett.*, *8*, 197–201.

Dekkers, M. J. (1988), Magnetic behavior of natural goethite during thermal demagnetization, *Geophys. Res. Lett.*, *15*, 538–541.

Dekkers, M. J. (1989a), Magnetic properties of natural goethite-I. Grain-size dependence of some low- and high-field related rock magnetic parameters measured at room temperature, *Geophys. J.*, *97*, 323–340.

Dekkers, M. J. (1989b), Magnetic properties of natural goethite-II. TRM behavior during thermal and alternating field demagnetization and low-temperature treatment, *Geophys. J.*, *97*, 341–355.

Dekkers, M. J., and P. Rochette (1992), Magnetic properties of CRM in synthetic and natural goethite: Prospects for a NRM/TRM intensity ratio test to assess the paleomagnetic stability for goethite, *J. Geophys. Res.*, *97*, 17,291–17,308.

Dunlop, D. J. (1982), Field dependence of magnetic blocking temperature: Analog tests using coercive force data, *J. Geophys. Res.*, *87*, 1121–1126.

Dunlop, D. J., and Ö. Özdemir (1997), *Rock Magnetism: Fundamentals and Frontiers*, Cambridge Univ. Press, New York.

France, D. E., and F. Oldfield (2000), Identifying goethite and hematite from rock magnetic measurements of soils and sediments, *J. Geophys. Res.*, *105*, 2781–2795.

Guyodo, Y., A. Mostrom, R. Lee Penn, and S. K. Banerjee (2003), From nanodots to nanorods: Oriented aggregation and magnetic evolution of nanocrystalline goethite, *Geophys. Res. Lett.*, *30*(10), 1512, doi:10.1029/2003GL017021.

Hedley, I. G. (1971), The weak ferromagnetism of goethite, *Z. Geophys.*, *37*, 409–420.

Heller, F. (1978), Rock magnetic studies of Upper Jurassic limestone of southern Germany, *J. Geophys.*, *44*, 525–543.

Kilkoyne, S. H., and C. Ritter (1997), The influence of Al on the magnetic properties of synthetic goethite, *Physica B*, *234–236*, 620–621.

Larrasoaña, J. C., A. P. Roberts, E. J. Rohling, M. Winklhofer, and R. Wehausen (2003), Three million years of monsoon variability over the northern Sahara, *Clim. Dyn.*, *21*, 689–698.

Liu, Q., J. Torrent, Y. Yu, and C. Deng (2004), Mechanism of the parasitic remanence of aluminous goethite [$\alpha$-(Fe, Al)OOH], *J. Geophys. Res.*, *109*, B12106, doi:10.1029/2004JB003352.

Maher, B. A., V. V. Karloukovski, and T. J. Mutch (2004), High-field remanence properties of synthetic and natural submicrometer haematites and goethites: Significance for environmental contexts, *Earth Planet Sci. Lett.*, *226*, 491–505.

Mathé, P. E., P. Rochette, and D. Vandamme (1999), Néel temperature of synthetic substituted goethites and their rapid determination using low-field susceptibility curves, *Geophys. Res. Lett.*, *14*, 2125–2128.

Özdemir, Ö., and D. J. Dunlop (1996), Thermal remanence and Néel temperature of goethite, *Geophys. Res. Lett.*, *23*, 921–924.

Pollard, R. J., Q. A. Pankhurst, and P. Zientek (1991), Magnetism in aluminous goethite, *Phys. Chem. Miner.*, *18*, 259–264.

Roberts, A. P., Y. L. Cui, and K. L. Verosub (1995), Wasp-waisted hysteresis loops: Mineral magnetic characteristics and discrimination of components in mixed magnetic systems, *J. Geophys. Res.*, *100*, 17,909–17,924.

Rochette, P., and G. Fillion (1989), Field and temperature behavior of remanence in synthetic goethite: Paleomagnetic implications, *Geophys. Res. Lett.*, *16*, 851–854.

Rochette, P., P.-E. Mathé, L. Esteban, H. Rakoto, J.-L. Bouchez, Q. Liu, and J. Torrent (2005), Non-saturation of the defect moment of goethite and fine-grained hematite up to 57 teslas, *Geophys. Res. Lett.*, *32*, L22309, doi:10.1029/2005GL024196.

Schulze, D. G., and U. Schwertmann (1984), The influence of aluminum on iron oxides: X. Properties of Al-substituted goethites, *Clay Miner.*, *19*, 521–539.

Schulze, D. G., and U. Schwertmann (1987), The influence of aluminum on iron oxides: XII. Properties of goethites synthesised in 0.3 M KOH at 25°C, *Clay Miner.*, *22*, 83–92.

Schwertmann, U. (1985), The effects of pedogenic environments on iron oxide minerals, *Adv. Soil Sci.*, *1*, 171–200.

Strangway, D. W., B. E. McMahon, and R. M. Honea (1967), Stable magnetic remanence in antiferromagnetic goethite, *Science*, *158*, 785–787.

Strangway, D. W., R. M. Honea, B. E. McMahon, and E. E. Larson (1968), The magnetic properties of naturally occurring goethite, *Geophys. J. R. Astron. Soc.*, *15*, 345–359.

Torrent, J., U. Schwertmann, and V. Barrón (1987), The reductive dissolution of synthetic goethite and hematite in dithionite, *Clay Miner.*, 22, 329–337.

Torrent, J., V. Barrón, and U. Schwertmann (1990), Phosphate adsorption and desorption by goethites differing in crystal morphology, *Soil Sci. Soc. Am. J.*, 54, 1007–1012.

―――――――――――

Q. Liu and A. P. Roberts, School of Ocean and Earth Science, National Oceanography Centre, University of Southampton, National Oceanography Centre, European Way, Southampton SO14 3ZH, UK. (liux0272@yahoo.com)

Y. Pan and R. Zhu, Paleomagnetism and Geochronology Laboratory (SKL-LE), Institute of Geology and Geophysics, Chinese Academy of Sciences, Beijing 10029, China. (rxzhu@mail.igcas.ac.cn)

Y. Yu, Department of Earth and Environmental Sciences, Korea University, South Korea.

J. Torrent, Departamento de Ciencias y Recursos Agrícolas y Forestales, Universidad de Córdoba, Edificio C4, Campus de Rabanales, E-14071 Córdoba, Spain.